Computational Exploration of a Pd(II)-Catalyzed γ-C–H Arylation where Stereoselectivity Arises from Attractive Aryl–Aryl Interactions

Katherine L. Bay,[1] Yun-Fang Yang,[1,2] K. N. Houk[1]*

[1]Department of Chemistry and Biochemistry, University of California, Los Angeles, CA 90095 USA

[2]College of Chemical Engineering, Zhejiang University of Technology, Hangzhou, Zhejiang 310014 P.R. China

ABSTRACT: The enantioselective Pd(II)-catalyzed γ-C–H arylation of picolinamides with a chiral BINOL phosphate ligand was explored using density functional theory (DFT). Enantioselectivity arises from attractive aryl–aryl interactions between the pseudo-equatorial phenyl substituent of the substrate and the chiral BINOL phosphate ligand.

Transition-metal catalysis is a powerful tool for aliphatic C–H functionalization.[1] While a number of enantioselective Pd(II)-catalyzed C–H desymmetrization processes have been reported by the Jin-Quan Yu group, there are few chiral ligands for asymmetric oxidative C–H functionalization with Pd(II) catalysts.[2] Chiral phosphines are incompatible with the reaction conditions needed for oxidative Pd(II)-catalyzed C–H functionalization.[3] Scheme 1 shows three examples of new classes of anionic chiral ligands that have been developed for Pd(II) catalysts that enantioselective C–H bond activations.

Yu *et al.* described a highly selective enantiotopic methylene C–H arylation in thioamide derivatives (Scheme 1a).[4] Gaunt *et al.* used a BINOL-phosphoric acid derivative to enable Pd-catalyzed enantioselective C–H amination of aliphatic amines to form aziridines (Scheme 1b). However, the role of the ligand has yet to be explained in either case.[5] Duan *et al.* used a BINOL-derived phosphoric acid and amide as ligands for aminoquinoline-directed benzylic β-C–H arylation of 3-arylpropanamides (Scheme 1c).[6]

Scheme 2 depicts a highly enantioselective picolinamide auxiliary-directed benzylic C–H arylation of 3-arylpropylamines that Gang He and Gong Chen *et al.* have reported recently.[7] This reaction requires (*R*)-BINOL phosphoric acid, Cs_2CO_3, and solvent-free conditions to produce the (*S*)-enantiomer of the product with up to 97% *e.e.* It has been known that Cs_2CO_3 is a highly soluble salt, which is essential since such reaction conditions are neat. We have investigated the role of the chiral ligand in controlling stereoselectivity. The experimentalists found the C–H activation step to be the rate- and stereoselectivity-determining step of the C–H aryl-

Scheme 1. Examples of Enantioselective Pd(II)-catalyzed C–H Activation Using Phosphine Ligands

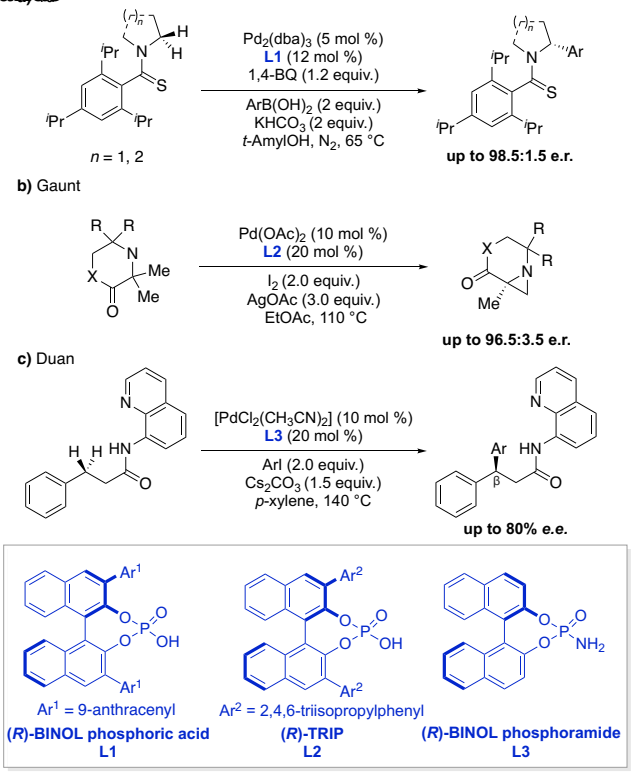

ation. Two different transition state models, A and B, were proposed as possible key concerted metallation deprotonation (CMD) C–H activation steps, involving either one **L** ligand or two **L** ligands bound by Cs^+ (Scheme 3). Based on observations of a non-linear

correlation between *e.e.* of **L** and *e.e.* of the product, it was proposed that multiple BINOL phosphate ligands might participate in the transition state.[7]

We used computations to differentiate between the two models and to elucidate the origins of enantioselectivity. In the two models developed, the role of the BINOL phosphate ligand differs at the transition state. In Model A, one phosphate ligand is responsible for both

Scheme 2. The He and Chen Enantioselective Pd-catalyzed Chiral Phosphate-mediated benzylic C–H Arylation Directed by a Picolinamide Auxiliary Group

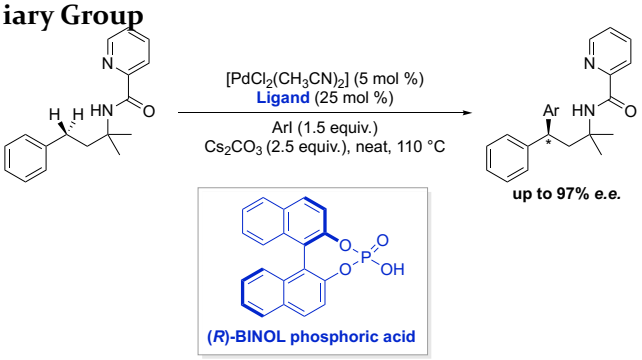

the metal coordination and hydrogen abstraction. However, in Model B one phosphate ligand coordinates as an anion to Pd, while the other phosphate ligand acts as an internal base for the hydrogen abstraction during the CMD step; here the phosphates are ion-paired to Cs^+. We also studied a truncated Model A without BINOL to establish the favored geometry of the transition state.

Scheme 3. Proposed Transition State Models for the Enantioselective C–H Palladation

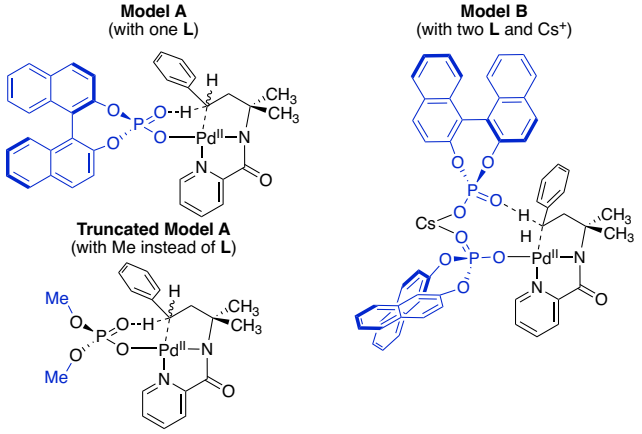

Quantum mechanical calculations were performed with Gaussian 09.[8] For Model A, geometries were optimized in the gas phase using the B3LYP[9] functional with the 6-31G(d)[10] basis set for all non-metal atoms and the LANL2DZ +f (1.472)[11] basis set with effective core potential (ECP) for Pd. Single point corrections were calculated using Truhlar's M06[12] functional with the 6-311++G(d,p)[13] basis set for all non-metal atoms and the SDD[14] effective core potential for Pd.

For Model B, ground state and transition state geometries were calculated using ONIOM(B3LYP[9]/6-31G(d)[10]-LANL2DZ[11]:UFF[15]) which enables optimizations of organometallic compounds with bulky ligands.[16] The BINOL ligands were calculated at the MM level while all the other atoms were calculated at the QM level. SCF (electronic) energies were obtained by single-point calculations using M06[13] functional with the 6-311++G(d,p)[13] basis set for all non-metal atoms and the SDD[14] effective core potential for Pd. Vibrational frequencies were computed at the QM:MM level to determine if the optimized structures are minima or saddle points on the potential energy surface corresponding to minima and transition state geometries, respectively. The reported free energies include zero-point energies and thermal corrections calculated at 298.15 K and 1 atm. Molecular structures are illustrated with CYLview.[17]

We studied the proposed catalytic cycle shown in Scheme 4. The computed barriers for each major step can be found in Supporting Information. The cycle starts with an activated Pd catalyst **A** as a bisligated species binding to the picolinamide substrate via N–H bond cleavage to form **B**. The γ-carbon of the substrate coordinates to Pd to form reactant complex **C**. Then, C–H activation occurs via CMD to form **D**. The neutral chiral phosphate ligand exchanges with MeCN to form **E**. Oxidative addition of iodotoluene occurs to form the Pd(IV) complex **F**, followed by reductive elimination **G** to form the arylated product. Computationally, it was found that the C–

Scheme 4. Proposed catalytic cycle for Pd-catalyzed C–H arylation of picolinamides

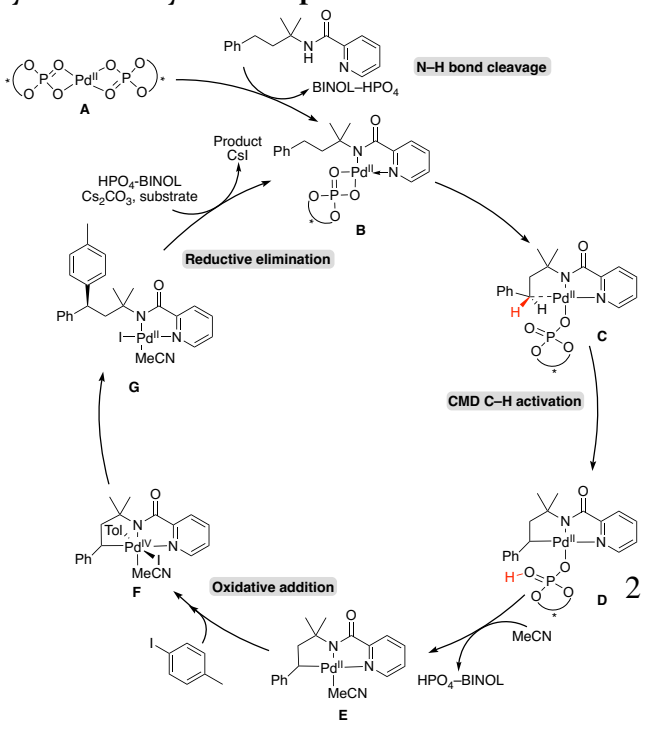

H activation step is the rate- and stereodetermining step, in accordance with experimental observations.

We first studied a simple model system, truncated Model A, in which the BINOL phosphate ligand in Model A is truncated to methyl substituents. The transition states for CMD are shown in Figure 1. The preferred conformation of the dimethyl phosphate is chiral, but the small methyl groups have minimal effect, so the (*S*) and (*R*) pseudo-equatorial TSs have slightly different energies. In **OMe TS(*S*)-2a** and **OMe TS(*R*)-4a**, there is a 1,3-diaxial interaction between the phenyl group and the closest methyl group, as seen in the Newman projection along the C_1–C_2 bond. This steric clash causes **OMe TS(*S*)-2a** to be 1.4 kcal mol^{-1} and **OMe TS(*R*)-4a** to be 1.5 kcal mol^{-1} higher in energy than **OMe TS(*S*)-1a**. The TS structure is lower in energy when the phenyl substituent is in the pseudo-equatorial position. We then used this information to build Model A with one chiral BINOL phosphate ligand and a phenyl substituent at the pseudo-equatorial position.

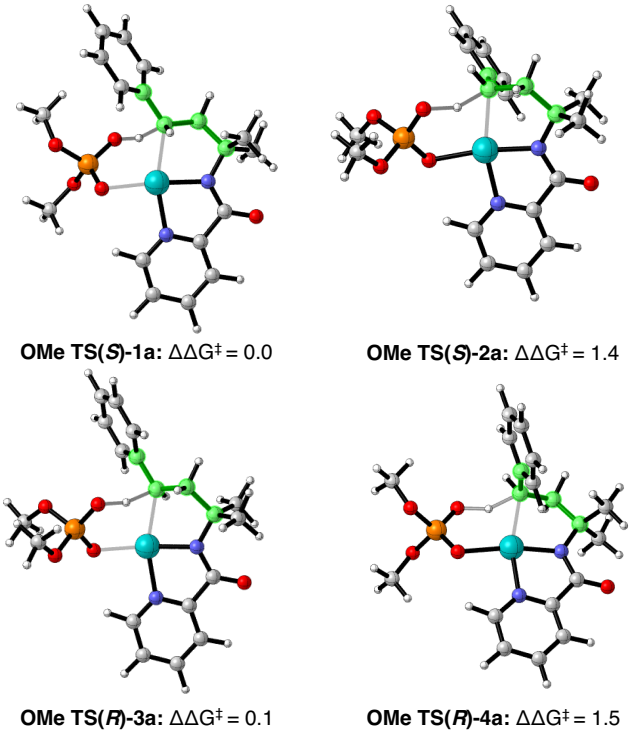

Figure 1. Conformers of CMD transition states of truncated Model A, where BINOL is replaced with methyl groups. Free energies are in units of kcal mol^{-1}.

Figure 2 shows the two lowest energy TS structures of Model A with one chiral phosphate BINOL ligand, **TS(*S*)-1a** and **TS(*R*)-2a**. The BINOL phosphate ligand, shown in blue in Figure 2 defines a plane, C_a–C_b–P. In **TS(*S*)-1a**, C_a–C_b–P is approximately coplanar with the square-planar Pd complex. However, in **TS(*R*)-2a** the C_a–C_b–P plane is rotated 90° about the C_2 axis and is perpendicular to the square-planar Pd complex. The binding mode of the BINOL phosphate ligand to Pd produces interactions that affect the enantioselectivity of the reaction.

The five-membered palladacycle, highlighted in blue on the right structure in Figure 2 puckers either above or below the palladacycle to form two different envelope conformations. Notably, both structures avoid steric clashes between the phenyl ring and methyl substituent by having the phenyl ring in the pseudo-equatorial position. **TS(*R*)-2a** is 3.2 kcal mol^{-1} higher in energy than **TS(*S*)-1a**.

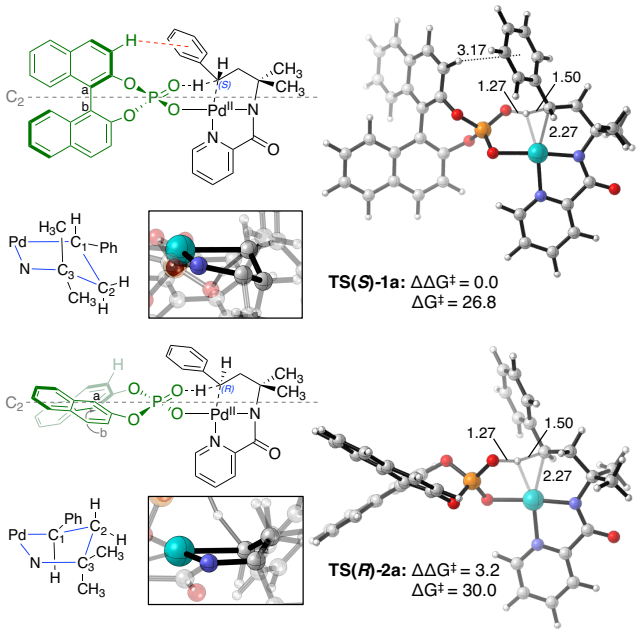

Figure 2. Optimized geometries of lowest energy transition states **TS(*S*)-1a** and **TS(*R*)-2a** for Model A involving one BINOL phosphate ligand. Distances and free energies are in units of Ångstroms and kcal mol^{-1}, respectively.

We surmise this energy difference is due to T-shaped interaction between the phenyl ring and the naphthyl substituent of the (*R*)-BINOL phosphate ligand. Experimentally, Chen *et al.* obtained 97% *e.e.* ($\Delta\Delta G^{\ddagger}$ = 2.8

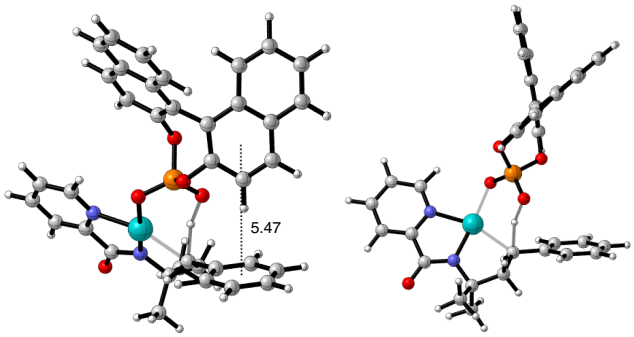

Figure 3. Edge-to-face aryl–aryl interaction in **TS(*S*)-1a**. Distances and free energies are in units of Ångstroms and kcal mol^{-1}, respectively.

kcal mol^{-1} at 110 ºC) in favor of the (*S*)-enantiomer from this reaction, which is in reasonable agreement with our computed results of $\Delta\Delta G^{\ddagger}$ = 3.2 kcal mol^{-1}. According to previous calculations, a C–H–π distance of 3.17 Å provides about 2.5 kcal mol^{-1} of stabilization in a benzene dimer.[18] **TS(*R*)-2a** does not have such C–H–π interactions because the ligand is bound perpendicular to the square-planar Pd complex. We analyzed the edge-to-face aryl–aryl interaction by measuring the distance from the center of one benzene ring to the center of the second benzene ring (Figure 3). This distance of 5.47 Å gives 2 kcal mol^{-1} stabilization for calculations on benzene dimers.[19] Both the C–H–π and edge-to-face aryl–aryl interaction is absent in the **TS(*R*)-2a**, the binding mode of the phosphate ligand is essential to the enantioselectivity.

Model B consists of two phosphate ligands bound by Cs^+. Details of the conformational analysis for the Cs-complex and the chiral catalyst are present in the Supporting Information. Figure 4 shows the lowest energy TS structures from Model B. Unlike Model A, **TS(*R*)-b** is only 0.8 kcal mol^{-1} higher in energy than **TS(*S*)-b**; Model B does not reproduce the experimentally observed level of selectivities of 97% *e.e.* In both **TS(*S*)-b** and **TS(*R*)-b**, the C_a–C_b–P plane of the ligand that participates in the H-abstraction is in the same plane of the

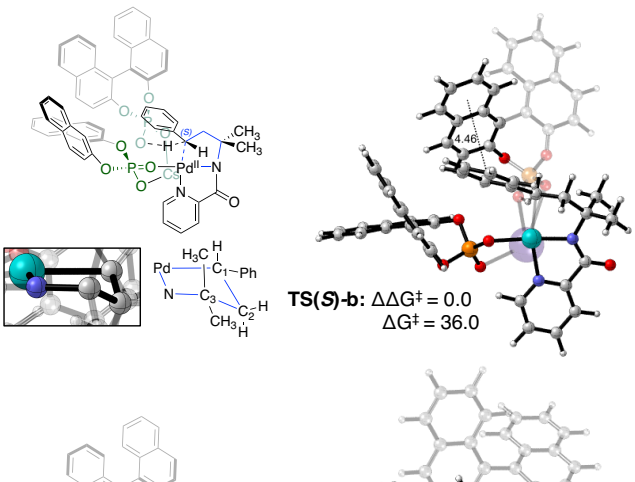

Figure 4. Optimized geometries of lowest energy transition states **TS(*S*)-b** and **TS(*R*)-b** for Model B involving two BINOL phosphate ligands. Bond distances and free energies are in units of Ångstroms and kcal mol^{-1}, respectively.

ligand coordinated to Pd is rotated such that it is perpendicular to the square-planar Pd-complex. The orientation square-planar Pd-complex; the C_a–C_b–P plane of the of both BINOL ligands around the phenyl ring increases the possibility for arene–arene interactions. All other ligand binding mode combinations that were explored with less arene–arene interaction gave higher energy transition states. This arises because the lowest-energy complexes both exhibit 5-membered palladacycles that minimize the possibility for steric clashes, since the phenyl substituent is in the pseudo-equatorial position. In both **TS(*S*)-b** and **TS(*R*)-b**, the phenyl ring is positioned between both BINOL ligands, allowing for π–π interactions to occur between the phenyl ring and the aromatic portions of the ligands. TS structures that did not exhibit such arene–arene interactions with the ligands were at least 3.0 kcal mol^{-1} higher in energy. The addition of another BINOL phosphate ligand in Model B allows for more stabilizing arene–arene interactions, which reduces the enantioselectivity.

In our mechanism, Cs^+ does not affect the CMD rate-determining TS, but the non-linear correlation between *e.e.* of **L** and *e.e.* of the product may arise from a BINOL phosphate ligand dimeric species bound by Cs^+ that is present off-cycle. This complex dissociates to form a monoligated species, serving as the activated catalyst **A**, as shown in our proposed mechanism. Since the reaction is run neat, Cs^+ may have additional non-catalytic roles.

We have elucidated the origins of the enantioselective palladium-catalyzed benzylic C–H arylation reaction of picolinamide-derivatized alkyl amines with aryl iodide.[8] The transition state involves a pseudo-

equatorial position of the phenyl substituent on the 5-membered palladacycle. When the ligand is positioned to abstract the H leading to the (*S*) product, there are stabilizing arene–arene interactions. The computed activation free energies ($\Delta\Delta G^{\ddagger}$) are consistent with experimental *e.e.*'s. Model A, proposed by Chen *et al.*, with one phosphate ligand, predicts the correct enantioselectivity, while Model B, with two phosphate ligands bound by Cs^{+}, predicts enantioselectivity that is much smaller than found experimentally. We anticipate that chiral catalysts with stabilizing arene–arene interactions can tune the enantioselectivity of C–H activation processes.

AUTHOR INFORMATION

Corresponding Author
***houk@chem.ucla.edu**

ACKNOWLEDGEMENTS

This work was supported by the National Science Foundation (CHE-1764320) and the National Science Foundation under the CCI Center for Selective C− H Functionalization (CHE-1700982). Computations were performed on the Hoffman2 cluster at UCLA and the Extreme Science and Engineering Discovery Environment (XSEDE), which is supported by the NSF (OCI-1053575). We also thank Prof. Gong Chen for helpful discussions regarding this work.

REFERENCES

[1] Yu, J.-Q.; Giri, R.; Chen, X. Org. Biomol. Chem. 2006, 4, 4041.

[2] Engle, K. M., Yu, J.-Q. *J. Org. Chem.* **2013**, *78*, 8927–8955.

[3] a) Anas, S.; Cordi, A.; Kagan, H. B. *Chem. Commun.* **2011**, *47*, 11483; b) Martin, N.; Pierre, C.; Davi, M.; Jazzar, R.; Baudoin, *O. Chem. - Eur. J.* **2012**, *18*, 4480; c) Saget, T.; Lemouzy, S.; Cramer, N. *Angew. Chem., Int. Ed*. **2012**, *51*, 2238; d) Yang, L.; Lucotti, A.; Tommasini, M.; Chalifoux, W. A. *J. Am. Chem. Soc*. **2016**, *138*, 9137; e) Saget, T.; Cramer, N. *Angew. Chem., Int. Ed.* **2012**, *51*, 12842; f) Pedroni, J.; Donets, P. A.; Cramer, N. *Chem. Sci*. **2015**, *6*, 5164; g) Nakanishi, M.; Katayev, D.; Besnard, C.; Kundig, E. P. *Angew. Chem., Int. Ed*. **2011**, *50*, 7438.

[4] Jain, P.; Verma, P.; Xia, G.; Yu, J.-Q. *Nat. Chem*. **2016**, *353*, 1023.

[5] Smalley, A. P.; Cuthbertson, J. D.; Gaunt, M. J. *J. Am. Chem. Soc.* **2017**, *139*, 1412.

[6] Yan, S.-B.; Zhang, S.; Duan, W.-L. *Org. Lett*. **2015**, *17*, 2458.

[7] Wang, H.; Tong, H.-R.; He, G.; Chen, G. *Angew. Chem., Int. Ed*. **2016**, *55*, 15387–15387.

[8] Frisch, M. J.; Trucks, G. W.; Schlegel, H. B.; Scuseria, G. E.; Robb, M. A.; Cheeseman, J. R.; Scalmani, G.; Barone, V.; Mennucci, B.; Petersson, G. A.; Nakatsuji, H.; Caricato, M.; Li, X.; Hratchian, H. P.; Izmaylov, A. F.; Bloino, J.; Zheng, G.; Sonnenberg, J. L.; Hada, M.; Ehara, M.; Toyota, K.; Fukuda, R.; Hasegawa, J.; Ishida, M.; Nakajima, T.; Honda, Y.; Kitao, O.; Nakai, H.; Vreven, T.; Montgomery, J. A.; Peralta, J. E.; Ogliaro, F.; Bearpark, M.; Heyd, J. J.; Brothers, E.; Kudin, K. N.; Staroverov, V. N.; Kobayashi, R.; Normand, J.; Raghavachari, K.; Rendell, A.; Burant, J. C.; Iyengar, S. S.; Tomasi, J.; Cossi, M.; Rega, N.; Millam, J. M.; Klene, M.; Knox, J. E.; Cross, J. B.; Bakken, V.; Adamo, C.; Jaramillo, J.; Gomperts, R.; Stratmann, R. E.; Yazyev, O.; Austin, A. J.; Cammi, R.; Pomelli, C.; Ochterski, J. W.; Martin, R. L.; Morokuma, K.; Zakrzewski, V. G.; Voth, G. A.; Salvador, P.; Dannenberg, J. J.; Dapprich, S.; Daniels, A. D.; Farkas; Foresman, J. B.; Ortiz, J. V.; Cioslowski, J.; Fox, D. J. *Gaussian 09*; Gaussian Inc.: Wallingford, CT, 2009.

[9] (a) A. D. Becke. *J. Chem. Phys.* **1993**, *98*, 5648–5652. (b) C. Lee, W. Yang, R. G. Parr. *Phys. Rev. B.* **1988**, *37*, 785–789. (c) A. D. Becke. *J. Chem. Phys*. **1993**, *98*, 1372–1377. (d) P. J. Stephens, F. J. Devlin, C. F. Chabalowski, M. J. Frisch. *J. Phys. Chem*. **1994**, *98*, 11623–11627.

[10] (a) R. Ditchfield, W. J. Hehre, J. A. Pople. *J. Chem. Phys.* **1971**, *54*, 724–728. (b) W. J. Hehre, R. Ditchfield, J. A. Pople. *J. Chem. Phys.* **1971,** *54*, 2257–2261.

[11] (a) P. J. Hay, W. R. Wadt. *J. Chem. Phys.* **1985**, *82*, 299–310. (b) L. E. Roy, P. J. Hay, R. L. Martin. *J. Chem. Theory Comput*. **2008**, *4*, 1029–1031. (c) A. W. Ehlers, M. Böhme, S. Dapprich, A. Gobbi, A. Höllwarth, V. Jonas, K. F. Köhler, R. Stegmann, A. Veldkamp, G. Frenking. *Chem. Phys. Lett*. **1993**, *208*, 111–114.

[12] Zhao, Y.; Truhlar, D. G. *Theor. Chem. Acc*. **2008**, *120*, 215.

[13] A. V. Marenich, C. J. Cramer, D. G. Truhlar. *J. Phys. Chem. B.* **2009**, *113*, 6378–6396.

[14] (a) M. Dolg, U. Wedig, H. Stoll, H. Preuss. *J. Chem. Phys.* **1987**, *86*, 866–872. (b) D. Andrae, U. Häußermann, M. Dolg, H. Stoll, H. Preu. *Theor. Chem. Acc.* **1990**, *77*, 123–141.

[15] (a) Morokuma, K. *et al. Chem. Rev*. **2015**, *115*, 5678–5796. (b) Dapprich, S., Komáromi, I., Byun, K. S., Morokuma, K. & Frisch, M. J. *J. Mol. Struct. (Theochem)*. **1999**, 462, 1–21. (c) Svensson, M. *et al. J. Phys. Chem.* **1996**, *100*, 19357–19363.

[16] Vreven, T. *et al. J. Chem. Theory and Comput.* **2006**, 2, 815–826.

[17] Legault, C. Y. CYLview, 1.0b; Université de Sherbrooke, 2009 (http://www.cylview.org).

[18] Tsuzuki, S.; Honda, K.; Uchimaru, T.; Mikami, M. *The Journal of Chemical Physics.* **2005**. *122*, 144323.
[19] Wheeler, S. E.; Houk, K. N. *Molecular Physics*, **2009**, *107*, 749–760.

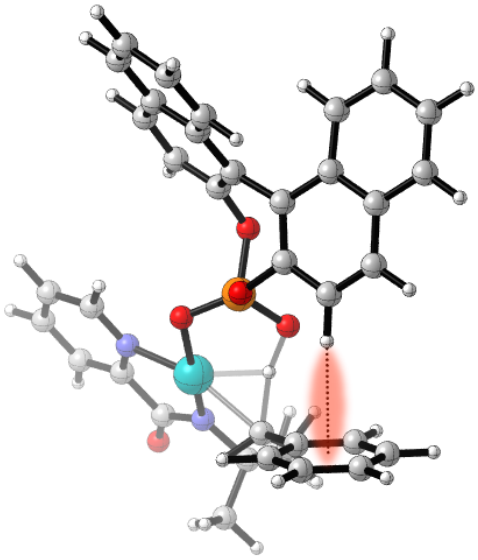

Enantioselectivity arises from attractive aryl–aryl interaction